Inorganic Chemistry

ARTICLE

pubs.acs.org/IC

Advances in the Chemistry of Nanosized Zirconium Phosphates: A New Mild and Quick Route to the Synthesis of Nanocrystals

Monica Pica,*[,†] Anna Donnadio,[†] Donatella Capitani,[‡] Riccardo Vivani,[†] Elisabetta Troni,[†] and Mario Casciola[†]

[†]Dipartimento di Chimica-CEMIN, University of Perugia, via Elce di Sotto 8, 06123, Perugia, Italy

[‡]Istituto di Metodologie Chimiche, Laboratorio di Risonanza Magnetica "Annalaura Segre", CNR, Via Salaria km 29.300, 00016 Monterotondo Scalo (RM), Italy

ABSTRACT: Simple addition of zirconyl propionate to phosphoric acid in alcoholic media surprisingly led to the formation, in few minutes, of transparent gels containing solvent intercalated zirconium phosphate (ZrP) nanoparticles with hexagonal shape and a planar size of about 40 nm. With the help of elemental analysis, inductively coupled plasma-optical emission spectrometry (ICP-OES), and ^{31}P magic angle spinning (MAS) NMR, the nanoparticle composition was formulated as $Zr(R)_w(HPO_4)_x(H_2PO_4)_y$, in which R can be an hydroxyl or a propionate group. The stoichiometric coefficients for propanol intercalated ZrP are $x = 1.43$, $y = 0.83$, and $w = 0.32$. Solvent elimination at 60 °C gave rise to an increase in the x value and a decrease in the y and w values. X-ray powder diffraction analysis and transmission electron microscopy (TEM) observations showed a concomitant increase in the particle size: planar size and thickness ranged from 90 to 200 nm and from 20 to 85 nm, respectively, depending on the nature of the solvent. A possible mechanism explaining the change in the x, y, and w values, the growth of nanoparticles, and the role of the solvent is proposed. Finally, the possibility of using these gels to disperse the ZrP nanoparticles within the polymer matrix of Nafion117 is shown.

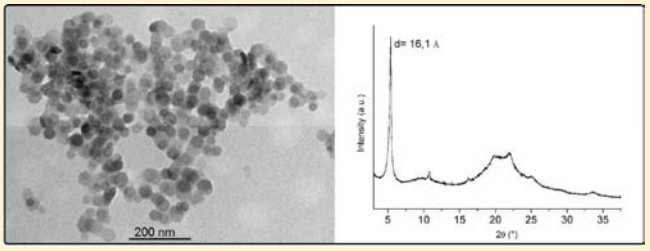

1. INTRODUCTION

Nowadays, the development of new compounds, as well as the reproducible preparation of known materials with specific chemical and physical properties, are of increasing importance. In particular, the expansion of the application range of the known functional materials needs the development of simple, mild, fast, and preferably clean synthetic routes, and the main role of a chemist is determining the most suitable conditions to obtain the product with the desired composition, structure, and properties. An important application field of inorganic materials, mainly those with a layered structure, includes polymeric nanocomposites.[1−3] These systems consist of an inorganic phase (filler) with at least one dimension in the nanometric scale, dispersed within a polymeric matrix. The filler−polymer interfacial interactions strongly affect the chemical, mechanical, and/or thermal properties of the matrix; consequently, a strict control of the chemical and morphological characteristics of the inorganic phase is required.

Besides clays, layered metal(IV) phosphates and phosphonates are well-known as fillers, as well as ion-exchangers, intercalation hosts, catalysts, and solid state proton conductors.[4−8] Among them, α-zirconium phosphates (hereafter ZrP) are undoubtely the most known and investigated ones. They have the same layer structure of α-type but can differ in the interlayer distances, water content, and/or different stacking sequence of the layers. Each α-layer is made of planes of zirconium atoms bonded, on both plane sides, to monohydrogen phosphate groups. Each phosphate group is bonded to three Zr atoms of the plane, while each zirconium is octahedrally coordinated by six oxygens of six monohydrogen phosphate groups. The water molecules can sit in the interlayer region forming a hydrogen-bonding network with the phosphate groups.[4,9]

The use of ZrP to prepare polymeric nanocomposites needs the total or partial exfoliation of the crystals which provides lamellar particles of nanometric thickness. So far the formation of colloidal dispersions of exfoliated ZrP has been achieved through the intercalation of suitable alkylamines in microcrystalline ZrP which results in the layer separation.[8,10−18] Moreover, a dense suspension (gel) of thin particles is obtained from these dispersions after the regeneration of the hydrogen form of ZrP.[14] While most of the approaches currently known to synthesize ZrP are based on the precipitation of the crystals at temperatures >80 °C, in the presence of concentrated acid solutions,[19−22] very few procedures allow precipitation of nanometric crystals in mild conditions[23,24] which, however, need one or more additional treatments to obtain intercalation compounds or colloidal dispersions.

Different from previous work, the present paper reports a one-pot synthetic route to prepare gels of nanosized ZrP intercalation compounds in aliphatic alcohols. The structural and physicochemical characterization of the gels and powders obtained after

Received: July 21, 2011
Published: October 20, 2011

solvent evaporation is also reported and discussed. Finally, the straightforward dispersion of the gels within a polymer solution is used for the preparation of a polymeric nanocomposite based on a perfluorosulfonic polymer.

2. EXPERIMENTAL SECTION

2.1. Chemicals. Zirconyl propionate ($ZrO_{1.26}(C_2H_5COO)_{1.49}$, MW = 220 Da) was supplied by Magnesium Elektron Ltd., England. Concentrated orthophosphoric acid (85%, 14.8 M) was supplied by Fluka. Anhydrous *n*-alkanols (ethanol, propanol, butanol) were purchased from Carlo Erba. Lanthanum hexaboride, LaB_6, was provided by The Gem Dugout, Deane K. Smith, 1652 Princeton Drive, State College, PA 16803. The Nafion dispersion (EW = 1100, 20 wt % in a mixture of aliphatic alcohols and water) and all other reagents were supplied by Aldrich.

2.2. Preparation of the ZrP Gels in Alcohol. In total, 3.3 mmol of zirconyl propionate was dissolved in 10 mL of anhydrous alcohol (ethanol, propanol, butanol). Concentrated phosphoric acid (0.45, 0.90, 1.35 mL) was added, at room temperature under stirring, to the above solution so that the H_3PO_4/Zr molar ratio (R) was 2, 4, and 6, respectively, and $[H_3PO_4] < 2$ M.

Clear solutions were obtained just after mixing which turned into gels in a few minutes. Transparent gels were obtained for $R > 2$. The gels thus obtained were washed three times with the same alcohol used for the synthesis in order to remove any excess of reagents (phosphoric acid) or byproduct (propionic acid). White powders were obtained by drying the gels in an oven at 60 °C until complete solvent elimination; the amount of ZrP in the gels ranged from 6 (with $R = 2$) to 8 (with $R = 6$) wt % ZrP. Hereafter the gel samples and powders obtained from the gels heated at 60 °C will be labeled as gel_alcohol_*R* and powd_alcohol_*R*, respectively, where "alcohol" is the solvent of the gel and "*R*" is the H_3PO_4/Zr molar ratio. By washing two times, gel_propanol_6 in DMF, a gel containing about 8 wt % ZrP, was obtained, which was used to prepare a Nafion/ZrP composite membrane.

2.3. Preparation of a Nafion/ZrP Composite Membrane. Typically, 5 g of the commercial Nafion dispersion was concentrated at 80 °C so as to reduce the volume by 90%. About 10 mL of DMF were added to the remaining solution, and the volume was reduced again. The procedure was repeated several times in order to ensure the complete removal of water and alcohols. The final dispersion contained about 15 wt % Nafion in DMF. A weighed amount of the ZrP gel in DMF was added to the Nafion dispersion in the same solvent, and the mixture was held under stirring at room temperature for about 15 min before casting on a Petri dish. A semitransparent membrane was obtained after solvent evaporation at 100 °C. Finally, the composite membrane was washed with a 1 M HCl solution at room temperature for 24 h and then heated at 80 °C for 4 h.

2.4. Techniques. X-ray powder diffraction (XRD) patterns were collected with a Panalytical X'Pert PRO diffractometer and a PW3050 goniometer equipped with an X'Celerator detector using the Cu−Kα radiation source with 2θ step size of 0.0170° and step scan of 60 s. The LFF ceramic tube operated at 40 kV, 40 mA.

To minimize preferred orientations, the powder samples were carefully side-loaded onto a glass sample holder, while gels were dropped and homogeneously distributed on an aluminum sample holder.

Solid state ^{31}P MAS NMR spectra were performed at 161.97 MHz on a Bruker Avance400 spectrometer. Gel samples were introduced into 4 mm zirconia rotors with an available volume reduced to 50 μL and sealed with Kel-F caps. The spin rate was set at 4 kHz, as a too high spin-rate destroys the gel. The $\pi/2$ pulse width was 3.5 s, the recycle delay was 40 s, and 400 scans were collected for each spectrum. After drying the gels, the obtained powders were packed into 4 mm zirconia rotors and sealed with Kel-F caps. The spin rate was 8 kHz. The $\pi/2$ pulse width was 3.5 s, and the recycle delay was 140 s; 1200 scans were collected for each spectrum. Spectra of gels were acquired using 4096 data points in the time domain, whereas spectra of powdered samples were acquired using 2048 data points. All spectra were zero filled and Fourier transformed. The chemical shift was externally referred to H_3PO_4 85%. The deconvolution of ^{31}P MAS spectra was performed using the DM2006 program.[25] The Gaussian/Lorentzian model was selected. Each resonance was characterized by the amplitude, the resonance frequency in parts per million (ppm), and the width at half-height.

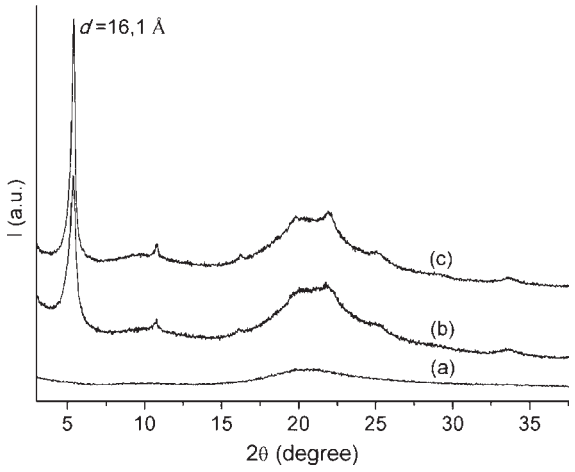

Figure 1. XRD patterns of gel_propanol_R samples, with $R = 2$ (a), 4 (b), and 6 (c).

Transmission electron microscopy (TEM) analysis was carried out by a JEOL JEM-2010 high-resolution transmission electron microscope, operating at an accelerating voltage of 200 kV. Fresh gel samples and powders were rapidly diluted in acetone in order to avoid aggregation phenomena, then supported on copper grids (200 mesh) precoated with a Formvar film, and quickly dried. The polymeric composite sample was first embedded in Araldite resin, then ultrathin sections of about 50 nm were cut at −80 °C by a Powertome-XL cryo ultramicrotome and placed on a 200 mesh copper grid.

Titration curves of solids dried at 60 °C were obtained by a radiometer automatic titrimeter (TIM900 Titrilab and ABU91 buret) operating at the equilibrium point method. Before titrations, the samples were equilibrated for 16 h, at room temperature, with a 1 M NaCl solution in order to exchange Na^+ ions for the protons of the solid. The solutions were then titrated under stirring with 0.1 M NaOH.

An ICP Varian Liberty inductively coupled plasma-optical emission spectrometry (ICP-OES) with axial injection was used for the quantitative analysis of zirconium and phosphorus. The samples to be analyzed were dried overnight in an oven at 60 °C, weighed, dissolved in 3 M HF ($\approx$ 2 mL), and diluted with water.

3. RESULTS AND DISCUSSION

3.1. Structural Characterization. Figures 1 and 2 show representative X-ray diffraction (XRD) patterns for gel_alcohol_*R* samples with $R = 2, 4, 6$ and alcohol = ethanol, propanol, butanol. The patterns essentially show only one strong reflection at low 2θ values and some weak higher order effects that appear for $R \geq 4$, whose position is independent of *R*. The *d* values of the first reflection correspond to the interlayer distance of microcrystalline ZrP intercalated with ethanol ($d = 14.4$ Å), propanol ($d = 16.1$ Å), and butanol ($d = 18.6$ Å), respectively, containing 2 mol of alcohol per mol of ZrP,[4] suggesting that the gels consist of crystalline domains of packed ZrP sheets.

dx.doi.org/10.1021/ic2015594 |*Inorg. Chem.* 2011, 50, 11623–11630

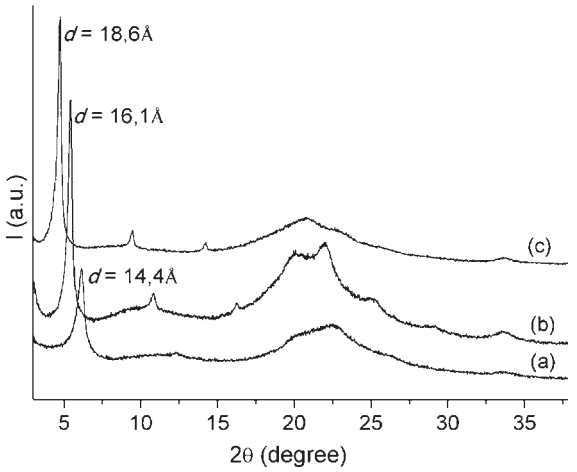

Figure 2. XRD patterns of gel_alcohol_6 samples, with alcohol = ethanol (a), propanol (b), and butanol (c).

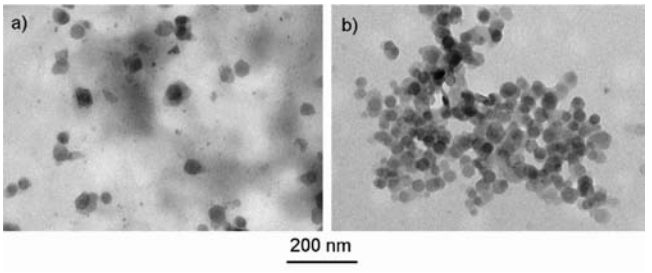

Figure 3. TEM images of gel_ethanol_4 (a) and gel_propanol_6 (b) samples.

Figure 3 shows the TEM images of gel_ethanol_4 (a) and gel_propanol_6 (b) samples. The presence of nanoparticles, with a regular planar size (about 40 nm) and nearly hexagonal shape is observed in both images indicating that planar size and morphology of the particles do not depend significantly on the solvent or on the *R* value used for their synthesis. Similar images were obtained for all other gel-samples.

When the gels were dried at 60 °C and stored at 53% relative humidity, giving rise to the powd_alcohol_*R* samples, the first reflection of each pattern shifted to d = 7.56 Å, and the whole pattern clearly indicated the formation of the monohydrated ZrP phase ($Zr(HPO_4)_2 \cdot H_2O$). Figure 4 shows representative XRD patterns of powd_propanol_*R* samples, while Figure 5 shows those of powd_alcohol_6 samples. The patterns are affected by a different broadening that reflects a different crystallinity and microstructure of samples. It clearly depends on the *R* value and on the alkanol used for the synthesis.

For R = 2 amorphous products were formed with all the solvents and compounds obtained with this molar ratio will not be considered later on. After drying, the nanoparticles kept their morphology, as revealed by the TEM image of the powd_alcohol_6 samples (Figure 6), although they showed a larger distribution of planar sizes, in the 30−200 nm range. The thickness of these particles is not easily deducible from TEM because of their preferential orientation in all the observed samples, probably due to the morphological anisotropy typical of layered compounds. This anisotropy is reflected in the XRD pattern as anisotropically broadened peaks, because the thickness

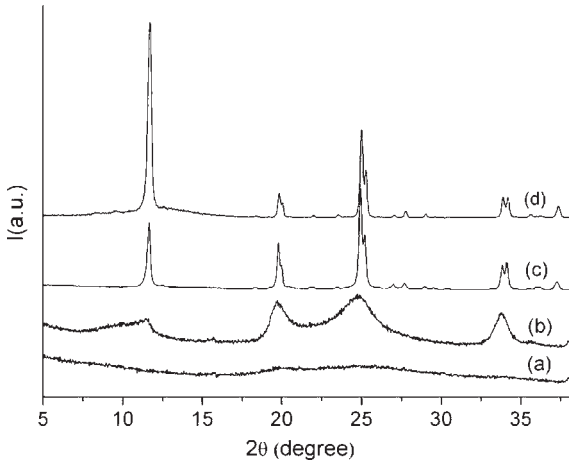

Figure 4. XRD patterns of the powd_propanol_*R* samples, with R = 2 (a), 4 (b), 6 (c), and microcrystalline α-ZrP (d).

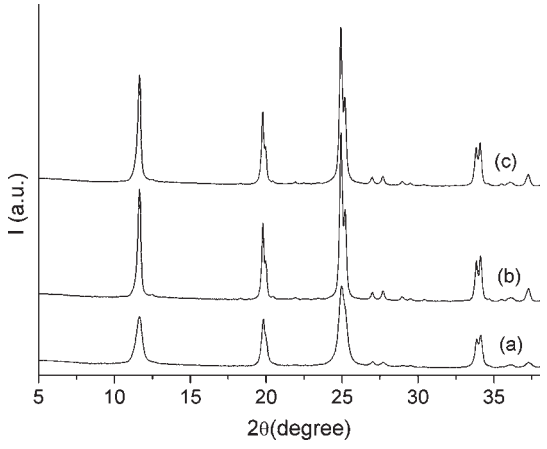

Figure 5. XRD patterns of the powd_alcohol_6 samples with alcohol = ethanol (a), propanol (b), and butanol (c).

of crystallite under the scattering plane is one of the main factors affecting the broadening of peaks. Therefore, for example, Bragg peaks coming from crystallographic planes perpendicular to the *c* axis (belonging to the 00*l* family) will be more broadened than others because in that direction the crystal is thinner.

Lattice defects, or microstrain, is another important factor that can affect diffraction peak broadening, especially in nanocrystals, where the interplanar distances can change between the core and the surface of particles and when the structure is highly defective. Also in this case, due to the structural anisotropy of ZrP, microstrain may produce an anisotropic broadening on the XRD pattern. Strain- and size-related contributions are different functions of the diffraction angle, so that it is possible to distinguish between the two effects.[26]

A third microstructural factor that may contribute to the whole broadening of Bragg peaks is the presence of stacking faults in the crystals. The modification of the diffraction peak profiles associated with the family of planes that contain these faults is similar to that caused by a size effect[27] and discrimination of these two contributions is not trivial: in this work we have neglected stacking fault effects. This approximation may overestimate the size-related contribution; therefore, we may consider that the obtained size values are minimum sizes. Nevertheless, to the best

dx.doi.org/10.1021/ic2015594 |*Inorg. Chem.* 2011, 50, 11623–11630

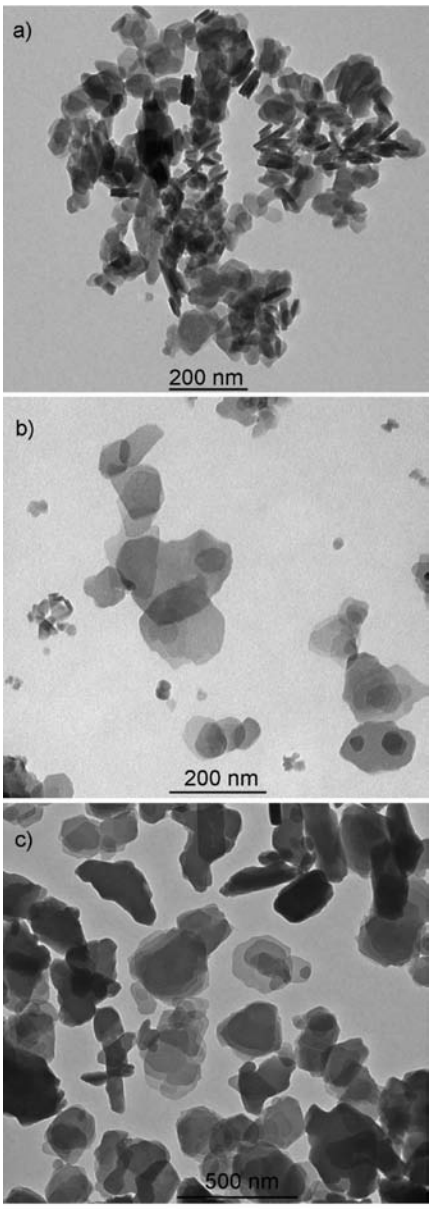

Figure 6. TEM images for the powd_alcohol_6 samples, with alcohol = ethanol (a), propanol (b), and butanol (c).

of our knowledge no scientific papers appeared in the recent literature reporting stacking fault studies in crystalline zirconium phosphates.

Structural and microstructural investigations were performed on the three powd_alcohol_6 samples with the Rietveld method using the GSAS-EXPGUI software package.[28] The structure of monohydrated ZrP[29] was adopted as the starting model. As discussed in the next section, the composition of powder samples slightly differs from that of microcrystalline compound, essentially due to phosphate coordination defects. Most of them are reasonably placed at the edge of nanocrystals. Because of this, and to an effective difficulty to account for these defects in the structural description of compounds, they were disregarded in the Rietveld refinement. Notwithstanding this, refinements with very good agreement factors were achieved. Figure 7 reports, as an example, the Rietveld plot for powd_propanol_6, showing the observed and calculated profiles and their difference.

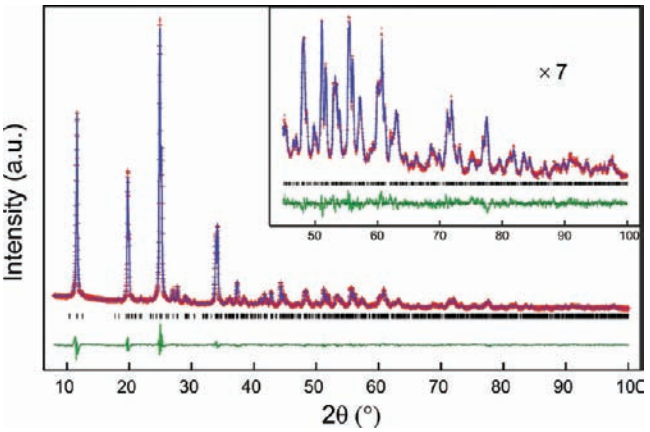

Figure 7. Rietveld plot of the last cycle of refinement for a powd_propanol_6 sample, showing the observed (red) and calculated (blue) profiles and their difference (green). Red marks indicate calculated positions of Bragg peaks.

Refined structural data are reported in Table 1 and are compared with those of a microcrystalline sample of monohydrated ZrP obtained by homogeneous precipitation from oxalic acid solutions.[29] The refinement involved scale factors, background coefficients, unit cell parameters, atomic positions, thermal factors, and profile-function parameters. No correction for preferred orientation was needed for nanocrystalline samples.

Unit cell parameters of different samples are similar to those of the microcrystalline homologous; however, all parameters (and therefore also the cell volume) tend to grow a little as the dimensions of crystallites decreases, when passing from the synthesis in butanol to propanol to ethanol. This effect may be due to an associated reduction of reticular energy.

The diffraction profile was modeled by a pseudo Voigt function as implemented in the GSAS package (profile function no. 3).[30] As expected, the profiles of patterns showed some anisotropy in the peak broadening that was modeled employing *Xe* and *Ye* anisotropic contributions to the peak-shape function, along the [001] anisotropic broadening axis. The instrumental contribution to the peak broadening was previously evaluated by the Rietveld refinement of the profile of lanthanum hexaboride, LaB_6, as an external peak profile standard. The refinement procedure was performed following the method described in ref 26. We assumed that the standard was not affected by microstrain, and the instrumental broadening was modeled by the refinement of *W* and *Y* peak shape parameters for Gaussian and Lorentzian contributions, respectively. For nanocrystalline compounds, refined peak shape parameters were *P*, *X*, and *Xe* that accounted for Gaussian and Lorentzian contributions to size effects and *U*, *Y*, and *Ye* for the corresponding microstrain effects, while *W* was fixed at the value refined on the standard. Two additional parameters for modeling asymmetry at a low angle were also refined.

The coherent domain sizes (volume-weighted) parallel and perpendicular to the *c* direction were estimated using the equations:

$$Dv_{\parallel} = 1800\lambda/\pi(X + Xe)$$

and

$$Dv_{\perp} = 1800\lambda/\pi X$$

dx.doi.org/10.1021/ic2015594 |*Inorg. Chem.* 2011, 50, 11623–11630

Table 1. Structural and Microstructural Data for powd_alcohol_6 Samples and for Monohydrated ZrP[29]

sample	powd_ethanol_6	powd_propanol_6	powd_butanol_6	monohydrated ZrP
a (Å)	9.0814(3)	9.0810(3)	9.0776(3)	9.0631(2)
b (Å)	5.2982(1)	5.2979(1)	5.2947(2)	5.2886(1)
c (Å)	15.4893(7)	15.4892(7)	15.4783(5)	15.4444(3)
β (deg)	101.722(4)	101.720(4)	101.720(3)	101.717(2)
V (Å)^3	729.73(3)	729.65(3)	728.43(2)	724.84(3)
$Dv_{\parallel}$ (nm)	23	65	85	140
$Dv_{\perp}$ (nm)	93	130	188	>400
$\varepsilon_{\parallel} \times 10^3$	6.5	2.5	6.6	5.0
$\varepsilon_{\perp} \times 10^3$	2.4	1.1	4.9	2.0
R_p[a]	1.97	1.99	3.42	4.31
R_{wp}[b]	2.52	2.55	4.53	6.27
R_F2[c]	2.29	2.27	5.80	7.88
GOF[d]	1.87	1.88	3.05	3.16

[a] $R_p = \Sigma|I_o - I_c|/\Sigma I_o$. [b] $R_{wp} = [\Sigma w(I_o - I_c)^2/\Sigma w I_o^2]^{1/2}$. [c] $R_F2 = \Sigma|F_o^2 - F_c^2|/\Sigma|F_o^2|$. [d] GOF $= [\Sigma w(I_o - I_c)^2/(N_o - N_{var})]^{1/2}$.

respectively, while the corresponding microstrain values were calculated with the following equations:

$$\varepsilon_{\parallel} = (\pi/18000)(Y + Ye - Yi)$$

and

$$\varepsilon_{\perp} = (\pi/18000)(Y - Yi)$$

in which Yi is the instrumental contribution, obtained by the refinement of the LaB_6 pattern.[28]

These results, reported in Table 1, show that coherent domain sizes along the *ab* plane ($Dv_{\perp}$) are roughly consistent with the average particle size observed by TEM. Analogously, we may assume that domain sizes along the *c* axis approximately correspond to the thickness of nanocrystals, from which moderate values of aspect ratio, ranging from 2 to 4, are obtained.

On the contrary, the domain size of the microcrystalline sample along the *ab* plane is very large, indicated as approximately >400 nm, and its contribution to the whole broadening is so small that it cannot be accurately evaluated.

General dimensions of powd-nanocrystals clearly depend on the solvent used for the synthesis, since they increase as the alkanol chain length increases and are larger than those of gel-samples (at least for planar sizes). In contrast, from TEM it seems that particle size of gel-samples do not depend on the alkanol used for their preparation. We have to deduce that the solvent should play its role during the drying process, when the system is transforming from a gel to a solid phase. In this stage, carried out at 60 °C in an oven, nanocrystals may fuse together and increase their size, thanks to the high reactivity of the surface and, in particular, edge of nanoparticles. This aggregation process probably becomes effective in the last stages of the drying treatment, when the particle density is high and some solvent is still present which can favor their mobility. At this stage, the alkanol may affect the evolution of the system, first because the time of drying (and therefore the available time for aggregation) strongly depends on the molar weight of the alkanol; moreover, we should recall that gels are made of layered nanocrystals intercalating alkanol molecules and deintercalation occurs only at the last stage of drying. Therefore, the alkanol may assist aggregation of nanocrystals, acting as templating agent through a van der Waals energy contribution that depends on alkanol chain length.

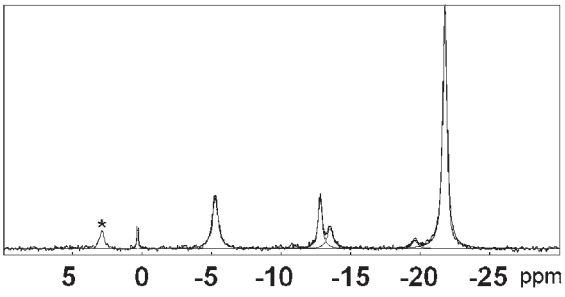

Figure 8. ^{31}P MAS NMR spectrum of a gel_propanol_6 sample; the resonance labeled with an asterisk is a spinning sideband.

Microstrain of samples shows an anisotropic behavior as well, and the values found in nanocrystals are very similar to those observed for microcrystalline monohydrate ZrP. Microstrain is significantly higher along the direction of packing, where covalent bonds alternate with van der Waals interactions.

3.2. NMR Characterization. Information about the local environment of phosphate groups was acquired by ^{31}P MAS NMR. The analysis of the NMR spectra of the gels revealed that these systems are more complex than expected. The spectrum of the sample gel_propanol_6 (Figure 8) shows six resonances at −21.82, −19.69, −13.58, −12.83, −5.28, and +0.31 ppm. Similar NMR spectra were obtained also for the other gel samples.

According to the literature,[31,32] resonances in the range −18.7 to −22.7 ppm are characteristic of monohydrogen phosphate groups bonded to three Zr(IV) atoms in the α-layer. Therefore, the resonances observed at −21.82 and −19.69 ppm are consistent with the α-type structure revealed by the XRD patterns.

As a result of the gel drying at 60 °C, the weak resonance at −19.69 ppm grows at the expense of the resonance at −21.82 ppm thus becoming the most intense signal of the spectrum (Figure 9). Similar changes were already observed for ZrP nanoparticles dispersed in Nafion 117 membranes[32] and were ascribed to an increasing size of the nanoparticles, which is actually observed by comparing Figures 3 and 6.

A further effect of the gel drying is the shift by −1/−2.5 ppm of the gel resonances in the range +0.31 to −13.58: in particular, the gel resonance at −5.28 ppm shifts to −7.93 ppm, while, as a

dx.doi.org/10.1021/ic2015594 |*Inorg. Chem.* 2011, 50, 11623–11630

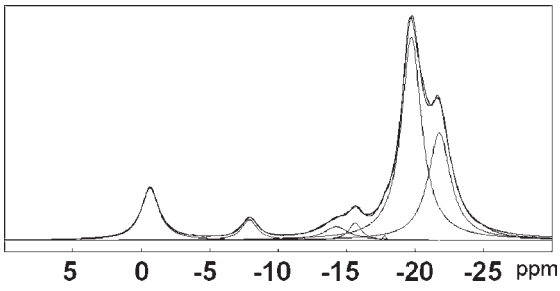

Figure 9. ^{31}P MAS NMR spectrum of a powd_propanol_6 sample.

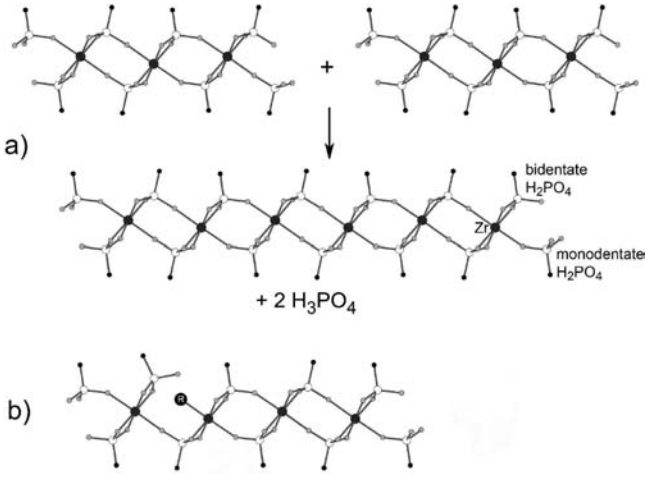

Figure 10. Schematic representation of (a) the growth of sheets with consequent elimination of phosphate excess at the edge of crystals and (b) coordination defects on the surface of ZrP sheets: a tridentate HPO_4 group is replaced by a bidentate H_2PO_4 and an R (OH or propionate) group.

consequence of the signal broadening, the gel resonances at −13.58 and −12.83 ppm give rise to a broad signal arising from the overlapping of resonances at −14.25 and −15.64 ppm. According to Benhamza[24] and Kapoor,[33] the signals at ≈ −5 (gel), −7 (powder) ppm and ≈ −12 (gel), −14 (powder) ppm can be assigned to H_2PO_4 groups bonded to Zr(IV) through one and two oxygen atoms, respectively.

Bulk structure of crystalline α-ZrP should contain only HPO_4 that are triple-connected to Zr; therefore, bi- or even monodentate phosphate groups must be located at the edge and corners of crystals or at least may represent coordination defects, in which a tridentate HPO_4 group is replaced by a bidentate H_2PO_4 and an R (hydroxyl or propionate) group. Both of these two conditions, schematically depicted in Figure 10, lead to a change in stoichiometry and involve the presence of H_2PO_4 groups.

Finally the resonances at +0.31 ppm for the gel and at −0.67 ppm for the powder are assigned to free phosphoric acid. The fact that the signal at +0.31 ppm is much sharper than the signal at −0.67 ppm is a clear indication that phosphoric acid is mainly present in the liquid phase of the gel while, in the powder, it is adsorbed on the ZrP nanoparticles.

The relative resonance areas for the gel and the powder, obtained by deconvolution, are listed in Table 2. It can be observed that after drying at 60 °C, the resonances assigned to

Table 2. Chemical Shifts (δ) and Resonance Areas of the ^{31}P MAS NMR Spectra for gel_propanol_6 and powd_propanol_6 Samples

gel			powder		
δ (ppm)	area (%)	assignment	δ (ppm)	area (%)	assignment
−21.82	60.24	HPO_4	−21.79	28.66	HPO_4
−19.69	1.70		−19.75	49.50	
−13.58	9.0	H_2PO_4	−17.79	0.14	
−12.83	10.24		−15.64	2.60	H_2PO_4
−5.28	16.92		−14.25	4.05	
0.31	1.87	H_3PO_4	−7.93	3.81	
			−0.67	11.22	H_3PO_4

H_3PO_4 and HPO_4 increase at the expense of the resonances of H_2PO_4: relative areas increase from 1.87% to 11.22% (+ 9.35%) for H_3PO_4 and from 61.94% to 78.30% (+16.36%) for HPO_4. The decrease of H_2PO_4 (mainly located at the edge) and the increase of H_3PO_4 and HPO_4 signals after gel drying, that is the increasing connectivity of the phosphate groups, are consistent with the growth of the particle size and the concomitant increase of the ratio (bulk groups)/(edge groups).[34] This process, also confirmed by TEM and XRD analysis, is depicted in Figure 10 and can be schematized as follows:

$$2H_2PO_4 \rightarrow H_3PO_4 + HPO_4$$

which however does not account quantitatively for the fact that the changes in the percentages of H_3PO_4 and HPO_4 are not equal. This can be explained by assuming that when the gel is dried at 60 °C some H_2PO_4 groups belonging to the coordination defects (Figure 10b) may react with the R groups, giving RH and HPO_4 groups that complete the coordination of adjacent Zr atoms.

On the basis of these considerations, the following general formula can be written for the gel and the powder:

$$Zr(R)_w(HPO_4)_x(H_2PO_4)_y \cdot zH_3PO_4$$

where R, besides being a hydroxyl group, could also be a propionate group ($-OOCCH_2CH_3$), which is present in the initial zirconyl propionate.

The coefficients *x*, *y*, *z*, and *w* are calculated taking into account the relative areas of the NMR signals and the total P/Zr molar ratio determined by ICP. The following compositions are obtained for the gel:

$$Zr(R)_{0.32}(HPO_4)_{1.43}(H_2PO_4)_{0.82} \cdot 0.045H_3PO_4$$

and for the powder:

$$Zr(R)_{0.16}(HPO_4)_{1.80}(H_2PO_4)_{0.24} \cdot 0.26H_3PO_4$$

3.3. Ion Exchange Characterization. To check the validity of the above formulas, the gel and the powder were titrated with 0.1 M NaOH. The titration curve of the gel cannot be used to this aim because it does not show well-defined inflection points. On the other hand, the titration curve of powd_propanol_6 (Figure 11) shows two rather sharp inflection points at pH = 4.5, corresponding to 3.84 mequiv of OH^-/g, and pH = 8.4 corresponding to 7.82 mequiv of OH^-/g. These values result from the contribution of the three different phosphate groups in the formula.

dx.doi.org/10.1021/ic2015594 |*Inorg. Chem.* 2011, 50, 11623–11630

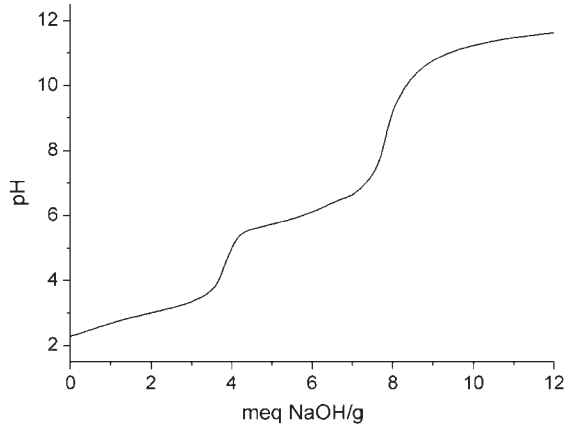

Figure 11. Titration curve of a powd_propanol_6 sample with 0.1 M NaOH.

In order to estimate these contributions the following considerations can be taken into account. First, the titration curve of microcrystalline α-$Zr(HPO_4)_2 \cdot H_2O$ suggests that 50% (0.9 mol per unit formula) of HPO_4 groups is neutralized at pH = 4.5, while all HPO_4 groups (1.8 mol) are neutralized at pH = 8.4.

The amount of protons belonging to H_2PO_4 that are titrated at pH $\leq$ 8.4 can be calculated by assuming that their ion exchange behavior in powd_propanol_6 is the same as in γ-$Zr(PO_4)(H_2PO_4) \cdot 2H_2O$,[35] since in both cases the H_2PO_4 groups are bonded to Zr through two oxygen atoms. On this basis, it can be inferred that 44% (0.21 mol) and 79% (0.38 mol) of the H_2PO_4 protons are neutralized at pH = 4.5 and pH = 8.4, respectively.

Finally, from the titration curve of H_3PO_4, it can be estimated that 33% (0.26 mol) and 65% (0.51 mol) of the protons of phosphoric acid are neutralized at pH = 4.5 and pH = 8.4, respectively.

Altogether, 1.37 and 2.69 protons per unit formula are expected to be titrated at the first and second inflection point, respectively. Then, assuming that in the above formula R is a propionate group and one hydration water molecule is present, the ion exchange capacity is 4.00 and 7.84 mequiv/g for the first and second inflection points, respectively, which is in good agreement with the experimental data.

3.4. Nafion/ZrP Composite Membranes. As already reported for ZrP gels obtained from exfoliated microcrystalline ZrP, the gel solvent can be easily replaced with alcohol miscible solvents by washing the gel with these solvents until alcohol elimination.[14] In particular gel_butanol_6 was repeatedly washed with DMF; as a consequence of butanol deintercalation and DMF intercalation, the first reflection of the XRD pattern shifted from d = 18.6 Å to d = 13.5 Å. This gel was expected to be suitable for dispersing α-ZrP nanoparticles in DMF soluble polymers, such as perfluorosulfonic ionomers, largely used as electrolytes in polymer electrolyte fuel cells. In this context, a Nafion/ZrP composite membrane containing 10 wt % ZrP was prepared by adding a suitable amount of the ZrP gel in DMF to a dispersion of the polymer in the same solvent. A semitransparent film was obtained by casting and subsequent solvent evaporation at 100 °C. The TEM image of the composite film (Figure 12) revealed that the filler particles are fairly homogeneously dispersed within the polymeric matrix and that their morphology is similar to that of the gel particles with a thickness of a few nanometers and a planar size of tens of nanometers.

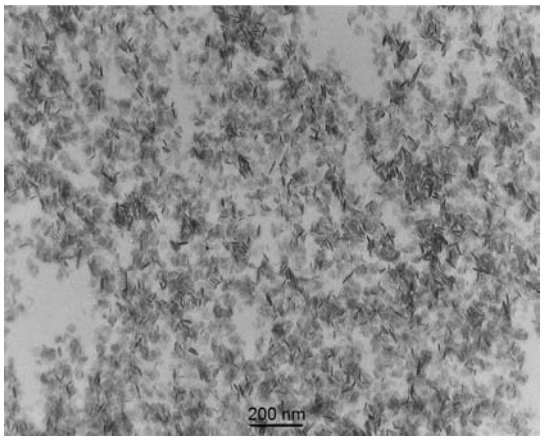

Figure 12. TEM image of a Nafion/10 wt % ZrP nanocomposite.

4. CONCLUSIONS

While amorphous ZrP is usually obtained by reacting an aqueous solution of a Zr(IV) salt with phosphoric acid, simple replacement of the aqueous solution with an alcoholic solution of zirconyl propionate leads to the formation of gels of nanocrystalline ZrP, consisting of hexagonal platelets with a size of some tens of nanometers. The XRD pattern of these gels revealed the direct formation of ZrP intercalation compounds with alcohols in the reaction medium, while the XRD analysis on the nanoparticle samples obtained after solvent eveporation showed the formation of larger ZrP nanocrystals with the α-layer structure. However, besides monohydrogen phosphate groups, solid state ^{31}P NMR spectra revealed the presence of dihydrogen phosphate groups, which are supposed to be located mainly at the particle edges.

Three main advantages come from the synthetic route reported in this paper: (1) the possibility to directly prepare ZrP nanometric particles by a one-pot reaction, at room temperature and without using highly concentrated acid solutions; (2) the possibility to directly obtain ZrP intercalation compounds with alcohols, which should make the exfoliation of the nanocrystals easier; and (3) the possibility of replacing the gel solvent with other solvents and to prepare dispersions of ZrP nanoparticles in a variety of polymer solutions, which can then be used to obtain polymer nanocomposites. In this connection, it has been shown that ZrP gels in DMF are suitable to obtain ZrP/Nafion nanocomposites where the filler particles keep the morphology of the particles of the starting gel.

AUTHOR INFORMATION

Corresponding Author

*E-mail: monica.pica@unipg.it. Phone: +39075 585 5564. Fax: +39075 585 5566.

ACKNOWLEDGMENT

This work was supported by Italian Ministry of University and Research (MIUR) under the PRIN 2007 Project.

REFERENCES

(1) Hussain, F.; Hojjati, M.; Okamoto, M.; Gorga, R. G. *J. Compos. Mater.* **2006**, *40*, 1511.

(2) LeBaron, P. C.; Wang, Z.; Pinnavaia, T. J. *Appl. Clay Sci.* **1999**, *15*, 11.
(3) Alexandre, M.; Dubois, P. *Mater. Sci. Eng.* **2000**, *28*, 1.
(4) Clearfield, A.; Costantino, U. In *Comprehensive Supramolecular Chemistry*; Alberti, G., Bein, T., Eds.; Pergamon, Elsevier Science Ltd. Press: New York, 1996; Vol. 7, Chapter 4.
(5) Alberti, G.; Casciola, M.; Pica, M.; Di Cesare, G. *Ann. N.Y. Acad. Sci.* **2003**, *984*, 208.
(6) Armento, P.; Casciola, M.; Marmottini, F.; Palombari, R.; Pica, M.; Ziarelli, F. *Solid State Ionics* **2004**, *4*, 19.
(7) Alberti, G.; Casciola, M.; Capitani, D.; Donnadio, A.; Narducci, R.; Pica, M.; Sganappa, M. *Electrochim. Acta* **2007**, *52*, 8125.
(8) Sue, H. J.; Gam, K. T.; Bestaoui, N.; Spurr, N.; Clearfield, A. *Chem. Mater.* **2004**, *16*, 242.
(9) Clearfield, A.; Smith, G. D. *Inorg. Chem.* **1969**, *8*, 431.
(10) Alberti, G.; Casciola, M.; Costantino, U. *J. Colloid Interface Sci.* **1985**, *107*, 256.
(11) Garcia, M. E.; Naffin, J. L.; Deng, N.; Mallouk, T. E. *Chem. Mater.* **1995**, *7*, 1968.
(12) Kim, H.-N.; Keller, S. W.; Mallouk, T. E.; Schmitt, J.; Decher, G. *Chem. Mater.* **1997**, *9*, 1414.
(13) Kaschak, D. M.; Johnson, S. A.; Hooks, D. E.; Kim, H.-N.; Ward, M. D.; Mallouk, T. E. *J. Am. Chem. Soc.* **1998**, *120*, 10887.
(14) Casciola, M.; Alberti, G.; Donnadio, A.; Pica, M.; Marmottini, F.; Piaggio, P.; Bottino, A. *J. Mater. Chem.* **2005**, *15*, 4262.
(15) Sun, L.; Boo, W. J.; Sun, D.; Clearfield, A.; Sue, H. J. *Chem. Mater.* **2007**, *19*, 1749.
(16) Boo, W.-J.; Sun, L.; Warren, G. L.; Moghbelli, E.; Pham, H.; Clearfield, A.; Sue, H.-J. *Polymer* **2007**, *48*, 1075.
(17) Boo, W. J.; Sun, L; Liu, J.; Moghbelli, E.; Clearfield, A.; Sue, H.-J.; Pham, H.; Verghese, N. *J. Polym. Sci., Part B: Polym. Phys.* **2007**, *45*, 1459.
(18) Bongiovanni, R.; Casciola, M.; Di Gianni, A.; Donnadio, A.; Malucelli, G. *Eur. Polym. J.* **2009**, *45*, 2487.
(19) Clearfield, A.; Stynes, J. A. *J. Inorg. Nucl. Chem.* **1964**, *26*, 117.
(20) Alberti, G.; Torracca, E. *J. Inorg. Nucl. Chem.* **1968**, *30*, 317.
(21) Sun, L.; Boo, W. J.; Sue, H. J.; Clearfield, A. *New J. Chem.* **2007**, *31*, 39.
(22) Willinger, M.-G.; Clavel, G.; Di, W.; Pinna, N. J. *Ind. Eng. Chem.* **2009**, *15*, 883.
(23) Bellezza, F.; Cipiciani, A.; Costantino, U.; Marmottini, F.; Quotadamo, M. A. *Colloid Polym. Sci.* **2006**, *285*, 19.
(24) Benhamza, H.; Barboux, P.; Bouhaouss, A.; Josien, F. A.; Livage, J. *J. Mater. Chem.* **1991**, *1*, 681.
(25) Massiot, D.; Fayon, F.; Capron, M.; King, I.; LeCalv, S.; Alonso, B.; Durand, J. O.; Bujoli, B.; Gan, Z.; Hoatson, G. *Magn. Reson. Chem.* **2002**, *40*, 70.
(26) Balzar, D.; Audebrand, N.; Daymond, M.; Fitch, A.; Hewat, A.; Langford, J. I.; Le Bail, A.; Louër, D.; Masson, O.; McCowan, C. N.; Popa, N. C.; Stephens, P. W.; Toby, B. *J. Appl. Crystallogr.* **2004**, *37*, 911.
(27) Guinebretière, R. *X-ray Diffraction by Polycrystalline Materials*; ISTE Ltd.: London, 2007.
(28) (a) Larson A. C.; Von Dreele, R. B. *General Structure Analysis System (GSAS)*, Los Alamos National Laboratory Report LAUR 86-748, 1994. (b) Toby, B. H. *J. Appl. Crystallogr.* **2001**, *34*, 210.
(29) Capitani, D.; Casciola, M.; Donnadio, A.; Vivani, R. *Inorg. Chem.* **2010**, *49*, 9409.
(30) (a) Thompson, P.; Cox, D. E.; Hastings, J. B. *J. Appl. Crystallogr.* **1987**, *20*, 79. (b) Finger, L. W.; Cox, D. E.; Jephcoat, A. P. *J. Appl. Crystallogr.* **1994**, *27*, 892.
(31) Clayden, N. *J. Chem. Soc., Dalton Trans.* **1987**, *8*, 1877.
(32) Casciola, M.; Capitani, D.; Comite, A.; Donnadio, A.; Frittella, V.; Pica, M.; Sganappa, M.; Varzi, A. *Fuel Cells* **2008**, *8*, 217.
(33) Kapoor, M. P.; Inagaki, S.; Yoshida, H. *J. Phys. Chem. B* **2005**, *109*, 9231.
(34) Tarafdar, A.; Panda, A. B.; Pradhan, N. C.; Pramanik, P. *Microporous Mesoporous Mater.* **2006**, *95*, 360.
(35) Clearfield, A.; Garces, J. M. *J. Inorg. Nucl. Chem.* **1979**, *41*, 879.